

International Conference on Space Optics—ICSO 2012

Ajaccio, Corse

9–12 October 2012

Edited by Bruno Cugny, Errico Armandillo, and Nikos Karafolas



Large micromirror array for multi-object spectroscopy in space

Michael Canonica

Frédéric Zamkotsian

Patrick Lanzoni

Wilfried Noell



Large micromirror array for Multi-Object Spectroscopy in space

Michael Canonica
EPFL
Neuchatel – Switzerland
(currently, MIT, Cambridge, USA)

Wilfried Noell
EPFL
Neuchatel – Switzerland

Frédéric Zamkotsian, Patrick Lanzoni
Laboratoire d'Astrophysique de Marseille (LAM)
Marseille – France
frederic.zamkotsian@oamp.fr

Abstract – Multi-object spectroscopy (MOS) is a powerful tool for space and ground-based telescopes for the study of the formation and evolution of galaxies. This technique requires a programmable slit mask for astronomical object selection.

We are engaged in a European development of micromirror arrays (MMA) for generating reflective slit masks in future MOS, called MIRA. The $100 \times 200 \mu\text{m}^2$ micromirrors are electrostatically tilted providing a precise angle. The main requirements are cryogenic environment capabilities, precise and uniform tilt angle over the whole device, uniformity of the mirror voltage-tilt hysteresis and a low mirror deformation.

A first MMA with single-crystal silicon micromirrors was successfully designed, fabricated and tested. A new generation of micromirror arrays composed of 2048 micromirrors (32×64) and modelled for individual addressing were fabricated using fusion and eutectic wafer-level bonding. These micromirrors without coating show a peak-to-valley deformation less than 10 nm, a tilt angle of 24° for an actuation voltage of 130 V. Individual addressing capability of each mirror has been demonstrated using a line-column algorithm based on an optimized voltage-tilt hysteresis. Devices are currently packaged, wire-bonded and integrated to a dedicated electronics to demonstrate the individual actuation of all micromirrors on an array. An operational test of this large array with gold coated mirrors has been done at cryogenic temperature (162 K): the micromirrors were actuated successfully before, during and after the cryogenic experiment. The micromirror surface deformation was measured at cryo and is below 30 nm peak-to-valley.

Keywords: MOEMS, MEMS, micromirror, large array, multi-object spectroscopy, cryogenic application, programmable slit mask.

I. INTRODUCTION

Large field of view surveys with a high density of objects such as high- z galaxies or stars benefit of multi-object spectroscopy (MOS) technique. Next-generation infrared astronomical instrumentation for ground-based and space telescopes could be based on MOEMS programmable slit masks for MOS. This astronomical technique is used

extensively to investigate the formation and evolution of galaxies. In order to optimize the Signal-to-Noise Ratio (SNR), the high precision spectra measurements could be obtained using a MOS. MOS with multi-slits is the best approach to eliminate the problem of spectral confusion, to optimize the quality and the SNR of the spectra, to reach fainter limiting fluxes and to maximize the scientific return both in cosmology and in legacy science. Major telescopes around the world are equipped with MOS in order to simultaneously record several hundred spectra in a single observation run. Next generation MOS for space like the Near Infrared Multi-Object Spectrograph (NIRSpec) for the James Webb Space Telescope (JWST) require a programmable multi-slit mask. Conventional masks or complex fiber-optics-based mechanisms are not attractive for space. The programmable multi-slit mask requires remote control of the multi-slit configuration in real time.

Micro-electro-mechanical systems (MEMS) have a great potential to provide field selector satisfying the most stringent requirements [1], [2], [3]. Different groups developed their own MEMS-based slit mask. The NASA's Goddard Space Center has developed Microshutter Arrays (MSA) for the multi-object spectrometer of the James Webb Space Telescope (JWST) [4]. During the early-phase studies of the European Space Agency (ESA) EUCLID mission, a MOS instrument based on a MOEMS device has been studied using the capabilities of the largest DMD in a space environment [5]. By placing the programmable slit mask in the focal plane of the telescope, the light from selected objects is directed toward the spectrograph, while the light from other objects and from the sky background is blocked. For example, a MOEMS-based MOS concept where the programmable slit mask is a MMA is shown in Fig. 1. In action, the micro-mirrors in the ON position direct the light toward the spectrograph, while the micro-mirrors in the OFF position are directing the beam towards a light trap.

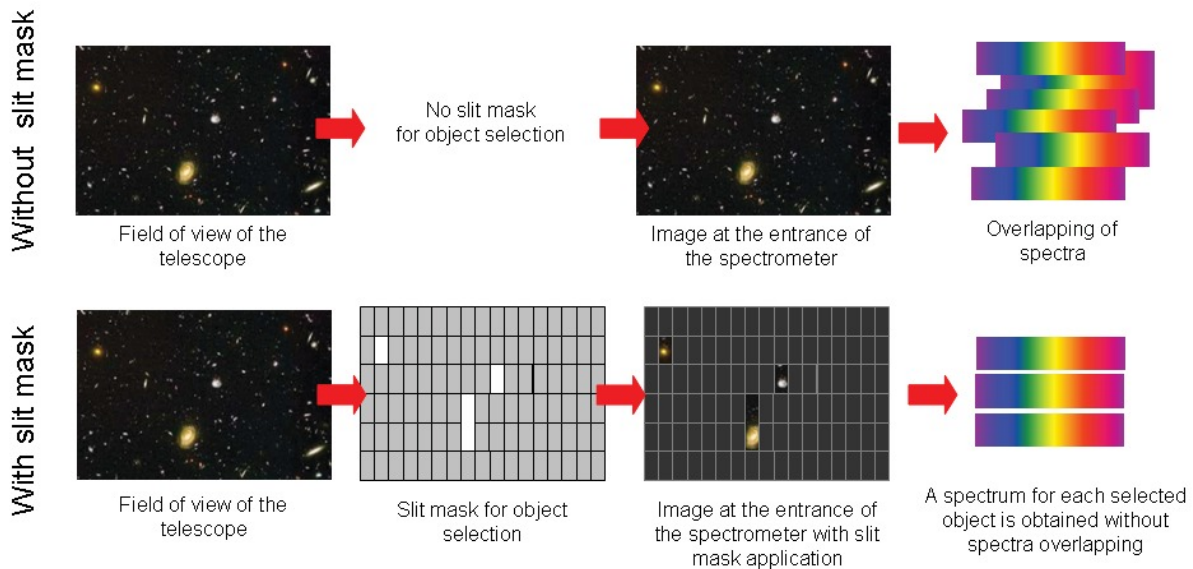


Figure 1. Multi-object spectroscopy requires a slit mask, for object selection, in the focal plane of the telescope. Object selection avoids overlapping of spectra and remove background signal.

Laboratoire d'Astrophysique de Marseille (LAM) and Ecole Polytechnique Fédérale de Lausanne (EPFL) began in 2004 a collaboration having the objective to develop a micromirror array (MMA) fully dedicated for multi-object spectroscopy [6], [7]. Our MMA has to achieve a mirror size of $100 \times 200 \mu\text{m}^2$, a mirror deformation lower than $\lambda/20$ ($\lambda = 1 \mu\text{m}$), a fill factor of more than 90 %, an optical contrast of 1000:1 (goal: 3000), a tilt angle of 20° , a tilt angle difference between mirrors lower than 10 arcminutes, an actuation voltage lower than 100 V, individual addressing capability of each micromirror, and finally it has to be cryogenic compatible.

In this paper, devices composed of 32×64 micromirrors with individual and line by line addressing capabilities were presented. These MMA were characterized electromechanically, optically and in a cryogenic environment. Finally, an individual actuation of 2×2 micromirrors was demonstrated.

II. CONCEPT

The micromirror was based on the electrostatic double plate actuator. A micromirror was suspended by two polysilicon flexion hinges, which were attached to a sustaining frame (Figure 2). To generate an electrostatic force, an electrode was placed underneath the micromirror and pillars were placed to set a precise electrostatic gap. A stopper beam was placed under the frame to set precisely the tilt angle of the micromirror after actuation. Finally, two landing beams were placed under the micromirror to avoid the micromirror to touch the electrode and generate short-circuits during the actuation.

When a voltage higher than the pull-in voltage was applied on the electrode, the micromirror was attracted by an electrostatic force towards the electrode. During this motion, it touched its stopper beam (Figure 2b) and landed on its landing pads. Therefore, after pull-in, the micromirror was electrostatically clamped at a precise tilt angle (Figure 2c). When the voltage was decreased, the micromirror took off from its stopper beam. When the restoring force of the flexure beams was higher than the electrostatic force the micromirror returned in its rest position.

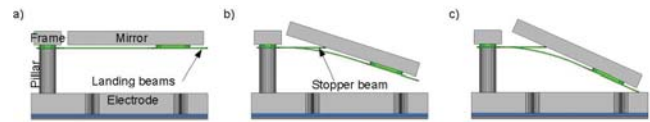


Figure 2. When a voltage was applied on the electrode, the micromirror was attracted towards its electrode by the action of an electrostatic force. During this motion, the mirror touched its stopper beam (b) and at the end of the motion, it was clamped at a precise tilt angle thanks to its contacts with its stopper beam and its landing pads (c).

The micromirrors were addressed of two different ways: line by line or individually. For line addressing, each line of micromirrors were directly connected to the electronics. On the other hand, for individual addressing due to the limited space available, it was not possible to connect each micromirror by an electrical connection. Therefore, individual addressing was implemented based on a line-column algorithm using the property of the tilt angle/voltage hysteresis [7]. This is a common technique in MEMS and it has been successfully applied e.g. to microshutter arrays [8].

For such actuation, the micromirrors were electrically connected along their lines while the electrodes were connected

in the perpendicular direction (Figure 3). Therefore, each micromirror of the array was addressed by setting the voltages of its line and of its column. To actuate individually several micromirrors of the array, the property of the tilt angle/voltage hysteresis was used. Indeed, the micromirror has two different tilt angles for the same actuation voltage. Therefore, using FEM simulation, micromirrors were modeled to possess a constant tilt angle after actuation, for voltages larger and lower than the pull-in voltage. Hence, when a tilted micromirror was placed at a voltage lower than the pull-in voltage, it was possible to actuate its neighboring micromirrors without changing its tilt angle.

When actuating a specific micromirror, we have to set the voltage along its line to V_{mir} and the voltage along its column to V_{el} . When the voltage difference between the line and the column is larger than the pull-in voltage ($V_{\text{p-in}}$), the mirror tilts to its operation angle.

The hysteresis behavior has the useful property, that – after pull-in has occurred - the operation angle can be kept at a voltage considerably lower than the pull-in voltage (Figure 3b, pos. 1 and pos. 3). Typically this means, that the voltage is decreased after pull-in without the actuator pulling out to its original rest position (pos. 1) but keeps its position in the same angle as at pull-in (pos. 3).

Therefore, to actuate a mirror having the position (m, n) in the array the following procedure is executed:

1. A voltage V_s is applied on the electrode n ($V_{\text{el}} = V_s$) to set the mirror into position 1.
2. A negative voltage δ is applied on the mirror line m ($V_{\text{mir}} = -\delta$). The voltage difference between the mirror and the electrode is larger than pull-in voltage ($V_{\text{el}} + V_{\text{mir}} > V_{\text{p-in}}$) and the mirror tilts into its operation angle (pos. 2).
3. The voltage on the mirror ($V_{\text{mir}} = 0$ V) is set to 0 V and the mirror moves into position 3 as desired.

At this point, if the neighboring mirror (m+1, n) has to be actuated we set the mirror line m+1 to the negative voltage δ , the mirror is in position 2, we set the mirror line m+1 at 0 and the mirror is in position 3. Finally, to recall all mirrors in their original rest position (pos. 0) we set the voltages for all electrodes and mirrors to 0V.

The procedure above allows actuating each micromirror of the array individually. Nevertheless, for successful application of the individual addressing concept, the position 3 of the hysteresis has to be as wide as possible, in order to compensate for non-uniformities of the electro-mechanical hysteresis among the micromirrors of the array

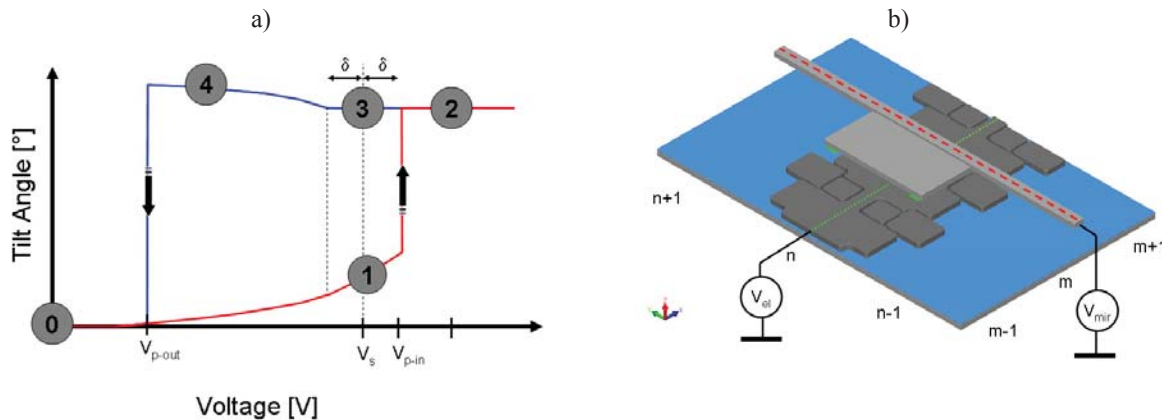


Figure 3. (a) Electrostatic voltage-tilt hysteresis of a micromirror with the relevant positions indicated. When the mirror is placed at the position 3, it stays with the operation tilt angle at a voltage lower than pull-in. (b) Design for addressing each micromirror of the MMA using a line – column algorithm based. The voltage of a line of micromirror and the voltage of a column of electrode can be set independently.

III. FABRICATION

Our MMA were microfabricated using bulk, surface micromachining and wafer level bonding. The electrode part and the mirror part were processed separately on different wafers and bonded together at the end of the process (Figure 4). A detailed description of the process was provided in reference [7].

The trenches surrounding the micromirrors were etched by DRIE in the device layer of the SOI wafer. These trenches were then covered by a 2 μm -thick layer of silicon dioxide by fusion bonding and thinning techniques. For the anchors of the beams, the silicon dioxide layer was etched by RIE. A polysilicon layer was deposited and patterned on the silicon dioxide layer to form the beams. The silicon dioxide layer was thinned down, patterned by RIE and a gold layer was deposited by lift-off technique. Finally, the silicon dioxide layer was completely etched.

For the electrode part, the two levels required on the surface (i.e. pillars and electrodes) were processed by DRIE delay mask process using a mask of silicon dioxide and a mask of photoresist.

The mirror part and the electrode part were then bonded by Au-Si eutectic bonding and the wafer stack was diced. The handle layer of the mirror wafer was then grinded at chip-level. The remaining silicon layer was patterned by honeycomb structures avoiding the bond between the pillars and the micromirror frame to break due to the stress generated by the BOX of the mirror wafer. Finally, the honeycomb structures were removed and the mirrors released by etching the BOX in HF vapor phase etcher.

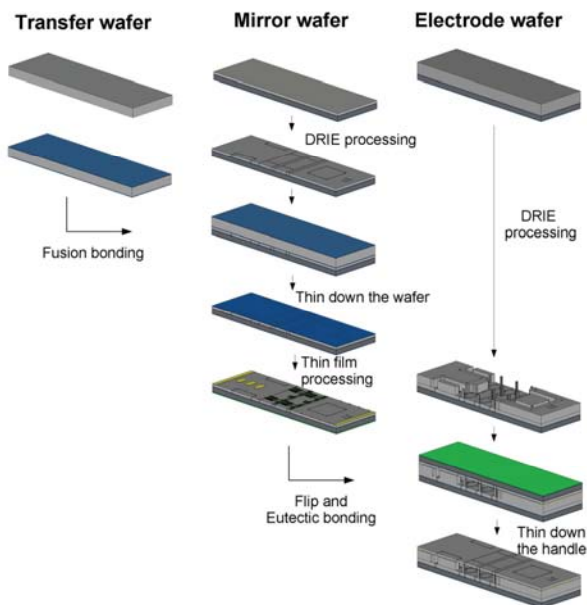


Figure 4: Fabrication process of the MMA involved three wafers and two wafer-level bonds. An oxidized transfer wafer was fusion bonded on top of the trenches of the mirror wafer. The transfer wafer was completely etched by grinding and KOH etching. The polysilicon beams and the gold pads were then patterned on the mirror wafer. Finally, the mirror wafer was bonded by Au-Si eutectic bonding on the DRIE-processed electrode wafer and the handle layer and the BOX of the mirror wafer were completely etched. The parts in grey represented the silicon parts, blue represented the silicon dioxide parts, green represented the polysilicon parts and yellow represented the gold parts.

After optimization of the process, fabrication of MMA was fully successful: No broken mirrors were observed (Figure 5). Moreover, this scalable process using wafer-level bonding was designed to make even larger arrays.

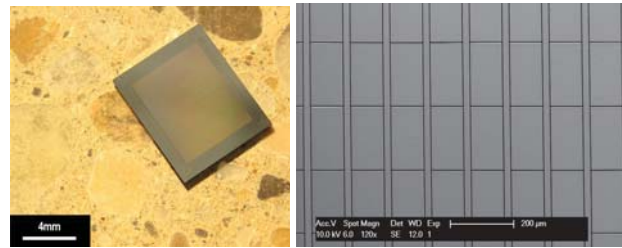


Figure 5: (a) Line addressed MMA of 2048 tilting micromirrors and measuring $10.5 \times 8.7 \text{ mm}^2$ dedicated for MOS. (b) Part of a MMA with micromirrors of $100 \times 200 \mu\text{m}^2$.

IV. CHARACTERIZATION

A. Tilt angle/voltage hysteresis

The tilt angle/voltage hysteresis was measured for a micromirror and compared with the FEM simulation computed with CoventorWare 2010 (Figure 6). For this characterization, a white light interferometer (Wyko NT1100 from Veeco) was coupled with a voltage supply. The voltage range was set from 0 to 140V and the tilt angle was measured every 2V.

From this measurement, the behavior of the micromirror was investigated. Before pull-in, the micromirror tilted of few degrees. At the pull-in voltage, the micromirror was attracted towards the electrode and was clamped at a precise tilt angle due to its stopper beam. When the voltage was decreased, the micromirror kept its tilt angle constant until 70V where it took off from its stopper beam increasing its tilt angle. When the restoring force of the flexure beams became larger than the electrostatic force, the micromirror returned in its rest position.

For this micromirror, pull-in occurred at a voltage of 120V and the tilt angle of the micromirror in its ON state was 25.3° . After pull-in, from 140 to 90V the micromirror varied its tilt angle of only 0.08° . Therefore, this design was well suited for line-column addressing because it had a tilt angle constant for a large voltage range below the pull-in voltage.

In comparison with the simulated values, the pull-in and pull-out of the micromirror were similar (within 5V). However, the tilt angle and the upper part of the hysteresis were not congruent with the simulation. These differences can be explained partly because fabrication process variations occurred modifying these features.

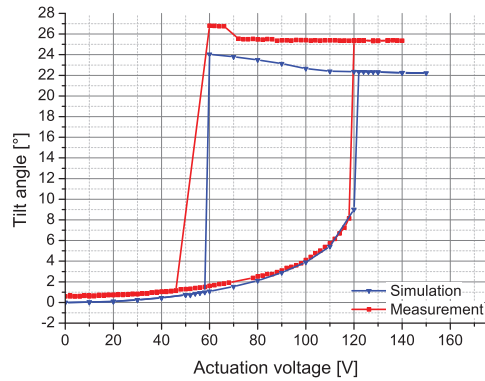


Figure 6. Micromirror tilt angle as a function of the actuation voltage. The measured data were obtained using a white light interferometer and the simulated data using the simulation software Coventorware 2010. The difference of tilt angle between the measured and the simulated data were probably due to fabrication process variation.

B. Fill factor

Although, the fill factor was mainly set during the modeling of the device, it varied as a function of the fabrication process. Therefore, the width of the trenches surrounding the micromirrors was characterized by SEM and the fill factor was calculated. A fill factor of 82.3% was obtained for the micromirror surface and of 98% in the direction along the length of the micromirror for the long slit mode.

C. Contrast

The contrast of a micromirror was characterized on a dedicated optical bench at LAM [9]. A light source having a diameter of 200 μm was focalized on a micromirror. Two pictures were recorded: for a micromirror at rest (OFF state) and for a micromirror tilted (ON state). The light intensity of each picture was integrated over the micromirror surface and the ratio between the pictures provided the contrast. Finally, for a micromirror tilting by 24°, a contrast ratio of 1000:1 was obtained.

D. Micromirror surface deformation

To increase the reflectivity for IR application, the silicon micromirrors were coated with gold. Since the micromirror deformation had to be as low as possible at room temperature and at cryogenic temperature, a study was undertaken to determine the coating inducing the smallest Peak-To-Valley (PTV) deformation. Two adhesion layers (Ti and Cr) for the gold layer were investigated. The micromirrors were measured by phase shift interferometry and the PTV deformation was obtained by taking the mean of the PTV deformation of the two diagonals of the mirror. For the first sample set, 30 silicon micromirrors of 10 x 100 x 200 μm^3 were measured without coating. Then, a coating of 10 nm of Ti and of 50 nm of Au was deposited on a single face of the mirror and the samples were measured.

Finally, the surface deformation induced by an adhesion layer of Cr was measured on other micromirrors coated with 10 nm of Cr and of 50 nm of Au.

The silicon micromirrors without coating demonstrated a PTV deformation of 5 nm (mean value). For an adhesion layer of Ti, a PTV deformation of 9.8 nm was obtained and of 11.9 nm for Cr (Figure 7). Therefore, using Ti rather than Cr as an adhesion layer demonstrated a little less of stress.

With a PTV surface deformation of about 10 nm, these micromirrors demonstrated an excellent quality and although the deformation may increase at cryogenic temperature, it should stay within the limit of 50 nm.

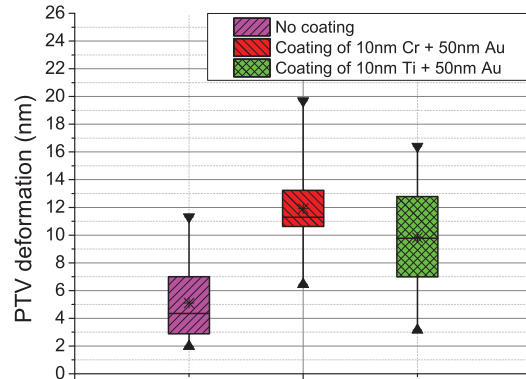


Figure 7: The PTV deformation was measured at room temperature for uncoated micromirrors, for mirrors coated with a layer of 10 nm of Ti and 50 nm of Au and for mirrors coated with 10 nm of Cr and 50 nm of Au. The mean value of the sample set for the uncoated micromirrors was 5 nm. With a coating of Ti, the deformation was 9.8 nm while for Cr it was 11.9 nm.

E. Cryogenic experiment

The cryogenic compatibility is crucial for the application in an infrared (IR) MOS. Our MMA is conceived such that all structural elements have a matched coefficient of thermal expansion (CTE) in order to avoid deformation or even flaking within the device when cooling down to the operating temperature. The mirrors themselves must be covered with a gold layer for IR operation, gold having a different CTE than silicon. As the silicon mirror is 10 μm thick and the coating 60nm thin, we estimate that the induced deformation will be small.

For characterising the surface quality and the performance of our MMA's at low temperature, we have developed a cryo chamber optically coupled to a high-resolution Twyman-Green interferometer [10]. The interferometer provides a sub-nanometer accuracy, and the cryo-chamber allows pressure down to 10⁻⁶ mbar and cryogenic temperatures. In order to get such temperature, the chamber is equipped with an internal screen insulating radiatively the sample from the chamber. Control of the

environment is obtained by means of temperature sensors and local heaters. They are wired to the outside environment through a Dutch connector and connected to a custom built control electronics.

The chamber has a glass window that allows observing and measuring the sample chip during cryogenic testing. The micromirror device is illuminated and imaged by a CCD camera on the outside; the micromirror device is rotated such that the light of the tilted mirrors (ON state) is sent to the CCD camera. The presence of a glass window at the entrance of the chamber is an issue for getting fringes with a high contrast.

Two elements have to be corrected:

- The path difference between the interferometer arms (sample arm and reference mirror arm).
- The glass medium is dispersive for the different wavelengths, each wavelength following a different path.

The first point could be overcome by moving the reference mirror in order to balance the path difference induced by the index difference between the window material and air, this balance is obtained for a very narrow linewidth. As we are using sources with low coherence, i. e. with a wide linewidth (typically 10nm), and as glass is dispersive, the path followed by each wavelength will be slightly different, degrading drastically the fringe pattern contrast. The only solution is to introduce in the reference arm a glass plate exactly identical to the window in the sample arm. The window and the reference plate have been ordered at the same time and installed on the bench. In Fig. 8 is given a view of the cryogenic chamber installed on our interferometric setup. The chamber is shown open during integration and closed when it is in operation.

The MMA device is packaged in PGA chip carrier. The PGA is inserted in a ZIF-holder integrated on a PCB board. Large copper surfaces on the PCB facilitate cooling down the system; renouncing the solder-stop layer eases outgassing of the PCB FR4 base material during evacuation of the chamber. The PCB itself is mounted via a fix-point-plane-attachment system to a solid aluminum block, the latter being interconnected to the cryo-generator. Thick copper wires between the PCB and the aluminum block further enhance thermal transport between the sample chip and the cryostat. A 100-pins feed-through connector links the chip with a custom built MMA control electronics. Temperature sensors are connected to the aluminum block and to the grid zip connector adjacent to the sample chip.

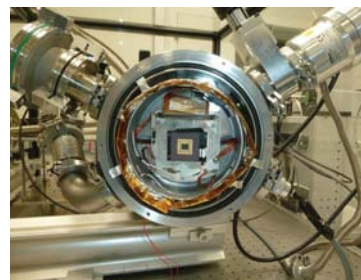


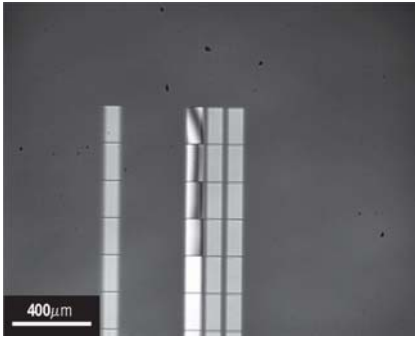
Figure 8: Views of the cryogenic chamber installed on our interferometric setup. The chamber is shown open during integration and closed when it is in operation. A MMA with 64 x 32 micromirrors is integrated, with 100 x 200 μm^2 micromirrors.

Before the cryogenic test, four lines of micromirrors were fully tilted at an actuation voltage of 130 V (Figure 9). The chamber was then cooled down to 162K, and under these conditions, 4 lines of 32 micromirrors were tilted at an actuation voltage of 148V. Nevertheless, some mirrors were not fully tilted because the actuation voltage was not high enough. Therefore, at cryogenic temperature the pull-in voltage increased as compared to the pull-in voltage at room temperature. Investigations are currently underway to understand the behavior of the MMA (doping level of the layers and local effects...).

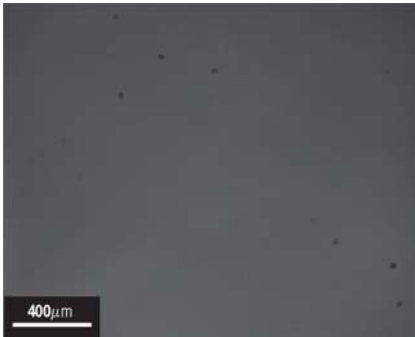
The micromirrors could be successfully actuated before, during and after cryogenic cooling at 162K. We could measure the surface quality of the gold coated micromirrors at room temperature and at 162 K without large deformation difference. Thanks to the use of a reference plate in the reference arm identical to the chamber window, we could get a high contrast in our measurements.

Interference fringes are clearly visible on the second column of actuated mirrors in Fig. 9, and we could then measure the mirror surface deformation when the device was actuated at room temperature and at cryogenic temperature. **A 9.8nm PTV surface deformation was measured at 293K, increasing up to 27.2nm PTV at 162K. When coming back at room temperature, we measured again the mirror surface deformation and obtained a value of 9.9nm PTV, identical to the value measured before cooling of the array.** The deformation is due to the CTE mismatch between the thick silicon micromirror and the thin gold coating layer on top. However, the surface deformation stays within the limit of 50 nm.

(a) Actuation of 4 lines of 32 micromirrors at 293K before the cryogenic experiment. An actuation voltage of 130V was applied. All the micromirrors tilted by 24°.



(b) Micromirrors at rest (OFF state) at 162K by setting the actuation voltage to 0V. No micromirrors are tilted.



(c) Actuation of 4 lines of 32 micromirrors (ON state) at 162K. An actuation voltage of 148V was applied and micromirrors tilted by 24°.

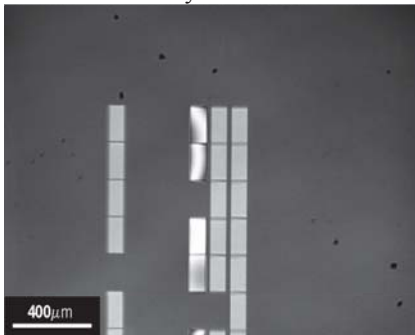


Figure 9. Interferometric observations of the lines of micromirrors before and during the cryogenic experiments. During this experiment, the cryogenic chamber was rotated of the value of the micromirror tilt angle. Therefore, the tilted micromirrors (ON state) appeared white on the Figure and the micromirror at rest, black (OFF state). Actuation of the micromirrors was demonstrated at 162K.

F. Line-column addressing 2 x 2

As a proof of concept of the individual addressing capabilities of the MMA, a 2 x 2 sub-part of a MMA of 32 x 64 micromirrors was actuated (Figure 10). For this demonstration, the line of micromirrors m was set to 80V, since the two electrodes were at ground the micromirror (m, n) and ($m, n+1$) tilted of few degrees. The electrode n was set to -30V, the voltage difference for mirror (m, n) became larger than the pull-in voltage and the micromirror tilted fully (Figure 11b). The electrode n was set to 0V and mirror (m, n) stayed tilted thanks to the tilt angle/voltage hysteresis. Then, the electrode $n+1$ was set to -30V and mirror ($m, n+1$) was fully tilted (Figure 11c). Again, the electrode $n+1$ was set to 0V and the micromirror stayed tilted. Following the same procedure, micromirror ($m+1, n$) was actuated, the line of micromirrors $m+1$ was set to 80V and its electrode n to -20V (Figure 11d). After actuation of mirror ($m+1, n$), the electrode n was set to 0V and the micromirror stayed tilted. To fully tilt mirror ($m+1, n+1$), the electrode $n+1$ was set to -10V. After the actuation of mirror ($m+1, n+1$) its electrode $n+1$ was set to 0V and the mirror stayed tilted. After the application of these voltages, the 4 micromirrors were fully tilted (Figure 11e). Finally, the voltages along the lines of micromirror m and $m+1$ were set to 0V and the 4 micromirrors returned to their rest position (Figure 11f). The pull-in voltage difference between these micromirrors occurred because for this device the frame was not fully assembled to the pillars changing locally the electrostatic gap.

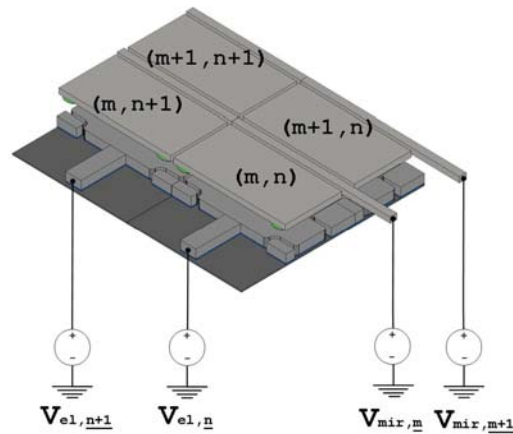
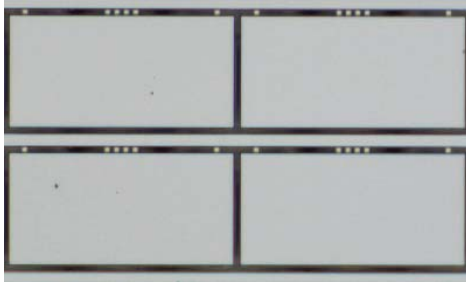
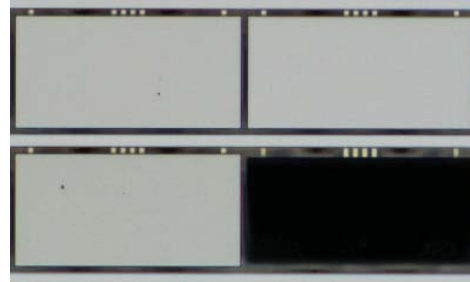


Figure 10. For the description of the line-column addressing capabilities of a 2 x 2 region, the line of micromirrors and their electrodes were indicated by letters.

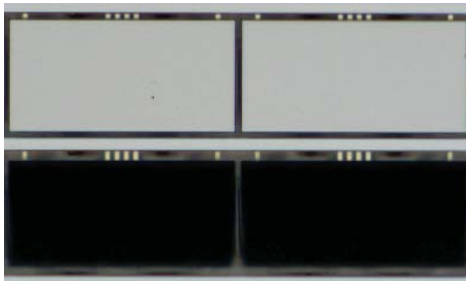
(a) All the mirrors were at rest because all the voltage sources were set at ground.



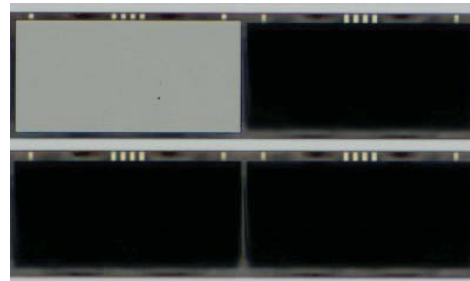
(b) Mirror (m, n) was tilted when its electrode n was set to 80V and its line to -30V.



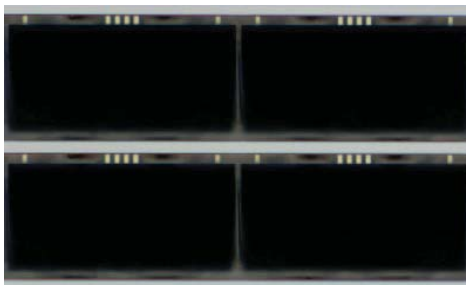
(c) Mirror $(m, n+1)$ was tilted when its electrode n was set to 80V and its line to -30V.



(d) Mirror $(m+1, n)$ was tilted when its electrode n was set to 80V and its line to -20V.



(e) Mirror $(m+1, n+1)$ was tilted when its electrode n was set to 80V and its line to -10V.



(f) All the mirrors were set at rest when the voltage sources were set at ground.

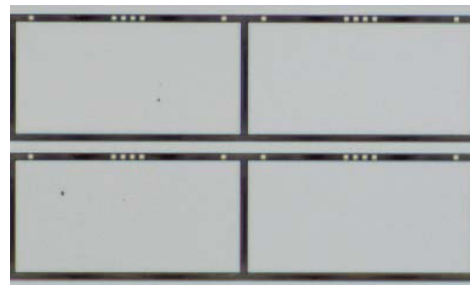


Figure 11. Demonstration of the line-column addressing capabilities of a 2 x 2 region of a 32 x 64 MMA. For this experiment, the device was not wire-bonded and probes were used to connect electrically the array. The pull-in voltage differences between these micromirrors can be explained because for this device the frame was not fully assembled to the pillars. The micromirrors measured $200 \times 100 \mu\text{m}^2$.

V. CONCLUSION

MMA for generating reflective slit masks in future MOS, called MIRA, were developed. MMA of 32 x 64 tilting 100 x 200 μm^2 micromirrors were successfully fabricated using three wafers and two wafer-level bonds (eutectic and fusion bonding). No broken micromirrors were observed on the final devices demonstrating the quality of the fabrication process.

The MMA were then characterized electromechanically, optically and in a cryogenic chamber. A tilt angle of 24° was measured for an actuation voltage of 130V. The fill factor characterized by SEM was 82.3% for the mirror surface and 98% in the direction along the micromirror lines. The contrast ratio between the rest and tilted state of the micromirror was 1000:1. The micromirrors coated with 10 nm of Ti and of 50 nm of Au showed a PTV surface deformation at room temperature of 9.8 nm. Several lines of 32 micromirrors were successfully tilted at a temperature of 162K. The micromirror surface deformation was measured at cryo and is as low as 27 nm PTV. Individual addressing of 4 micromirrors was demonstrated using a line-column algorithm based on the tilt angle/voltage hysteresis of the electrostatic actuator. Line-column addressing of arrays of 2048 micromirrors are currently under investigation.

MIRA prototype demonstrates the ability of such MOEMS device to work as objects selector in future generation of MOS instruments both in ground-based and space telescopes.

VI. ACKNOWLEDGEMENTS

We gratefully acknowledge the Division C staff at CSEM (Centre Suisse d'Electronique et de Microtechnique) and the CMI (Center of Microtechnology) staff at EPFL, for their support during the fabrication of the devices. We also acknowledge the SNF R'Equip program for the funding of the data acquisition test bench for Microsystems, (RF)MEMS and NEMS used in this study. Finally, we acknowledge the staff of "Service Essais" at LAM during the tests at cryogenic temperature.

REFERENCES

- [1] R. Burg, P.Y. Bely, B. Woodruff, J. MacKenty, M. Stiavelli, S. Casertano, C. McCreight and A. Hoffman, "Yardstick integrated science instrument module concept for NGST", in *Proceedings of the SPIE conference on Space Telescope and Instruments V*, SPIE **3356**, 98-105, Kona, Hawaii, 1998
- [2] F. Zamkotsian, K. Dohlen, D. Burgarella, V. Buat, "Aspects of MMA for MOS: optical modeling and surface characterization, spectrograph optical design", in *Proceedings of the NASA conference on "NGST Science and Technology Exposition"*, ASP Conf. Ser. **207**, 218-224, Hyannis, USA, 1999
- [3] M. Robberto, A. Cimatti, A. Jacobsen, F. Zamkotsian, F. M. Zerbi, "Applications of DMDs for Astrophysical Research", in *Proceedings of the SPIE conference on MOEMS 2009*, Proc. SPIE **7210**, San Jose, USA (2009)
- [4] M. J. Li; A. D. Brown; A. S. Kutuyev; H. S. Moseley; V. Mikula, "JWST microshutter array system and beyond", Proc. SPIE 7594, San Francisco, USA, 2010
- [5] F. Zamkotsian, P. Lanzoni, E. Grassi, R. Barette, C. Fabron, K. Tangen, L. Valenziano, L. Marchand, L. Duvet " Successful evaluation for space applications of the 2048x1080 DMD," in *Proceedings of the SPIE conference on MOEMS 2011*, Proc. SPIE **7932**, San Francisco, USA (2011)
- [6] S. Waldis, F. Zamkotsian, P.-A. Clerc, W. Noell, M. Zickar, N. De Rooij, "Arrays of high tilt-angle micromirrors for multiobject spectroscopy, " *IEEE Journal of Selected Topics in Quantum Electronics* **13**, pp. 168–176 (2007).
- [7] M. Canonica, S. Waldis, F. Zamkotsian, P. Lanzoni, W. Noell, and N. De Rooij, "Realization and characterization of a MEMS-based programmable slit mask for multi-object spectroscopy," Proc. SPIE **7594**, (2010)
- [8] M. E. McNie, A. G. Brown, D. O. King, G. W. Smith, N. T. Gordon, S. Riches, and S. Rogers, "A 2x2 multi-chip reconfigurable MOEMS mask - A stepping stone to large format microshutter arrays for coded aperture applications," Proc. SPIE **7818**, (2010)
- [9] F. Zamkotsian, J. Gautier, P. Lanzoni, "Characterization of MOEMS devices for the instrumentation of Next Generation Space Telescope," in *Proceedings of the SPIE conference on MOEMS 2003*, Proc. SPIE **4980**, San Jose, USA (2003)
- [10] A. Liotard, F. Zamkotsian, "Static and dynamic micro-deformable mirror characterization by phase-shifting and time-averaged interferometry", in *Proceedings of the SPIE conference on Astronomical Telescopes and Instrumentation 2004*, Proc. SPIE **5494**, Glasgow, United Kingdom (2004)